Nanoscale

PAPER

View Article Online
View Journal | View Issue

Cite this: *Nanoscale*, 2024, **16**, 2466

Functional magnetic nanoparticles for protein delivery applications: understanding protein–nanoparticle interactions†

Rajat Sharma, [a] Daniel Ungar, [b] Edward Dyson, [c] Stephen Rimmer [c] and Victor Chechik *[a]

Received 8th September 2023,
Accepted 20th December 2023

DOI: 10.1039/d3nr04544g

rsc.li/nanoscale

Iron oxide nanoparticles (IONPs) surface functionalised with thermo-responsive polymers can encapsulate therapeutic proteins and release them upon heating with an alternating magnetic field above the lower critical solution temperature (LCST). In order to make this delivery system clinically-relevant, we prepared IONPs coated with poly-*N*-isopropylmethacrylamide (PNIPMAM), a polymer with LCST above human body temperature. The optimal polymer chain length and nanoparticle size to achieve LCST of *ca.* 45 °C were 19 kDa PNIPMAM and 16 nm IONPs. The PNIPMAM-coated IONPs could encapsulate a range of proteins which were released upon heating above LCST in the presence of a competitor protein or serum. A small amount of encapsulated protein leakage was observed below LCST. The efficiency of protein encapsulation and release was correlated with molecular weight and glycosylation state of the proteins. Magnetic heating resulted in a faster protein release as compared to conventional heating without significant temperature increase of the bulk solution.

1. Introduction

Stimuli-responsive nano-assemblies have attracted significant attention, due to their ability to undergo controlled morphological or functional changes.[1–3,6,8] Heat is a particularly attractive trigger as it can be easily applied either directly with good spatiotemporal control, or indirectly through photothermal or magneto-thermal effects.[8] Many examples of thermo-responsive polymer assemblies for heat-triggered drug release applications have been reported.[1–3,8] For instance, some polymers undergo fast and reversible phase transition from a swollen to a collapsed state at the lower critical solution temperature (LCST), which could trigger release of an encapsulated guest molecule. This thermo-responsive behaviour can be combined with magnetic iron oxide nanoparticles (IONPs), which are able to generate heat in the presence of alternating magnetic field (AMF). Polymer-coated IONPs thus can be used to release the encapsulated guest locally at the targeted sites.[8]

The best studied material of this type of application is poly(*N*-isopropylacrylamide) (PNIPAM). However, the LCST of the PNIPAM polymer (*ca.* 32 °C) is below the human body temperature hindering *in vivo* drug delivery application.[8] The LCST can be increased by co-polymerisation with hydrophilic monomers such as acrylamide. For instance, poly(*N*-isopropylacrylamide-*co*-acrylamide)-*block*-polyethylene imine coated IONPs provided heat-triggered release of doxorubicin at 39 °C.[2] Moreover, nanocomposite membranes based on nanogels (LCST *ca.* 40 °C) and magnetite IONPs achieved "on-demand" drug delivery upon the application of an oscillating magnetic field.[3] In this case the nanogel was a co-polymer of *N*-isopropylacrylamide, acrylamide and *N*-isopropylmethacrylamide. The latter monomer can also be used to make a homo-polymer, poly(*N*-isopropylmethacrylamide) (PNIPMAM), which has an LCST of *ca.* 42 °C.[4,5] As PNIPMAM only differs from PNIPAM in one methyl group in its repeat unit, similar drug encapsulation/triggered release behaviour to PNIPAM could be expected.

Most reports on polymer-coated IONPs are focussed on the delivery and release of small molecules.[6,7] Encapsulation of therapeutic proteins is less explored. Recently, we reported successful protein encapsulation and magneto-thermal release from 10 kDa PNIPAM coated 6 nm IONPs.[8] With conventional heating, the protein cargo was released above the LCST in the presence of a competitor protein. Importantly, AMF selectively heated the core of IONPs and magnetic heating-triggered protein release could be observed at bulk solution temperatures below the LCST (*ca.* 21 °C). This proof-of-principle study showed successful delivery of the growth factor Wnt3a in a functional form to the mesenchymal stem cells (MSCs). Wnt3a release from coated IONPs resulted in significant increase of cell proliferation.

[a]*Department of Chemistry, University of York, UK. E-mail: victor.chechik@york.ac.uk*
[b]*Department of Biology, University of York, UK*
[c]*Polymer and Biomaterials Chemistry Laboratories, University of Bradford, UK*
† Electronic supplementary information (ESI) available. See DOI: https://doi.org/10.1039/d3nr04544g

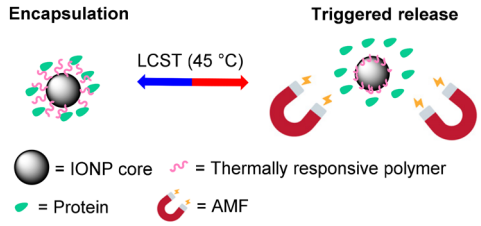

Scheme 1 Schematic illustration of the protein release from the thermally-responsive polymer-coated IONPs using magnetic heating as a trigger.

Here, building on our previous findings, we report construction of PNIPMAM coated IONPs that can release a cargo protein above 45 °C (Scheme 1). The particle size and morphology of IONPs have been optimised to enable efficient heating by AMF. We also show that protein size and glycosylation state are important determinants for encapsulation and competitive release of cargo proteins.

2. Results and discussion

2.1. PNIPMAM synthesis and characterization

Thermally responsive PNIPMAM polymers were synthesized *via* RAFT polymerization with azobisisobutyronitrile (AIBN) as a radical initiator and *S*-1-dodecyl-*S*′-(α,α′-dimethyl-α″-acetic acid)trithiocarbonate as a chain transfer agent (CTA) (Scheme 2).[9,10] Polymer with the smallest average molecular weight M_w was characterised by matrix assisted laser desorption ionization mass spectrometry (MALDI-MS) (Fig. 1(i)). The expanded spectrum revealed a repeating set of peaks separated from neighbouring sets by the monomer mass (127 Da), which confirmed the successful synthesis of PNIPMAM. MALDI MS spectra of polymers with higher M_w > 10 kDa were too weak. Gel permeation chromatography (GPC) analysis showed that polymer size distribution (Fig. 1(ii)) was broad, presumably due to insufficient removal of oxygen during polymerisation. Nonetheless, both free polymer and polymer-coated nanoparticles showed good phase transition properties in the desired temperature range (*vide infra*).

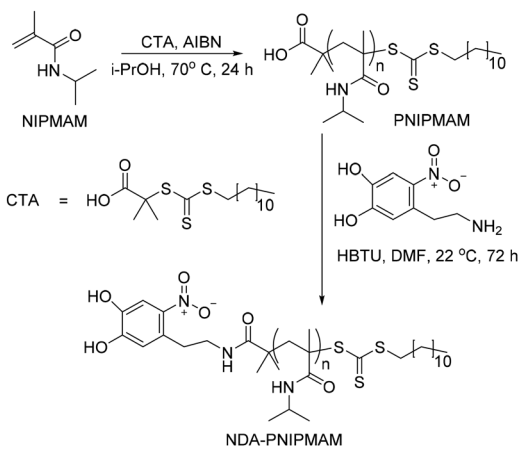

Scheme 2 RAFT polymerization and end group modification to give NDA end group PNIPMAM.

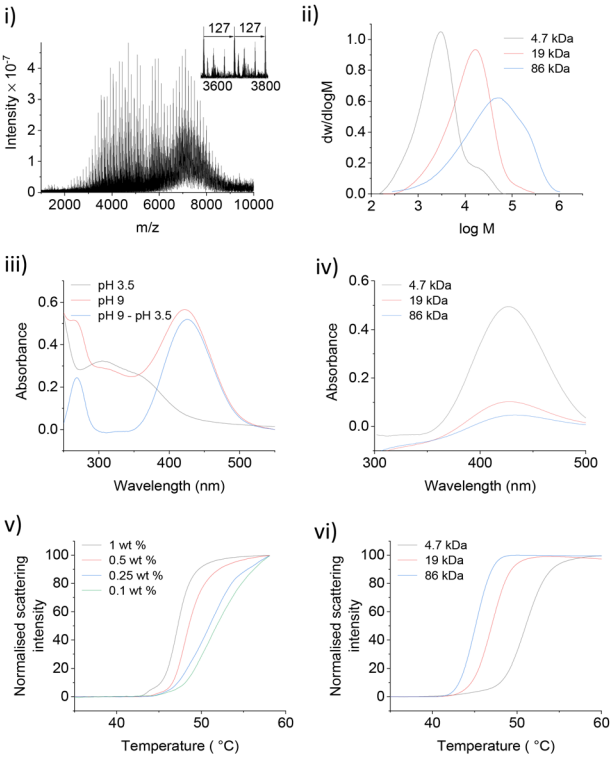

Fig. 1 (i) MALDI-MS spectra of 4.7 kDa NDA-PNIPMAM. (ii) GPC chromatograms of NDA-PNIPMAM. (iii) UV-Vis spectra of 4.7 kDa NDA-PNIPMAM at pH 3.5 and 9 with and without using the pH 3.5 spectrum as a baseline. (iv) UV-Vis spectra of different NDA-PNIPMAM polymers at pH 9 (pH 3.5 as baseline). (v) NanoDSF traces of 19 kDa NDA-PNIPMAM at different concentrations (in 10 mM TRIS, pH = 7). (vi) NanoDSF traces of different NDA-PNIPMAM polymers (0.5 mM in 10 mM TRIS, pH = 7).

To facilitate the attachment of PNIPMAM to the IONPs, the end group of the polymer was functionalised with 6-nitrodopamine (NDA), which is a commonly used catechol anchor for iron oxide.[11] It can be attached to the PNIPMAM polymer chains either before (pre-functionalisation) or after polymerisation (post-functionalisation).[12,13] We used the post-functionalisation approach because it allows incorporation of functionalities incompatible with the polymerisation process.[11] Functionalisation with NDA was carried out by coupling the acid terminal group of the polymer to the amine functionality of NDA using HBTU as a coupling agent (Scheme 2). MALDI-MS confirmed complete disappearance of the original polymer peaks and the appearance of a new set of NDA functionalized polymer peaks consistent with the conversion of PNIPMAM to NDA-PNIPMAM (Fig. S1.1†).

Since both the thiocarbonylthio and NDA end groups are UV active, the resultant polymer was characterised by UV-Vis spectroscopy (Fig. 1(iii)). The shoulder corresponding to the thiocarbonylthio group (308 nm) confirmed its presence in the

functionalised polymer (Fig. 1(iii)).[14] The UV spectrum of NDA-PNIPMAM showed a nitrocatechol peak at 350 nm (λ_{max}) at acidic pH (below the 1st p$K_a \approx 7$ of the nitrocatechol group), which shifted to the visible range (*ca.* 422 nm) at pH 9. Free NDA also showed peaks at the same positions. Using a pH 3.5 UV spectrum as a background for the pH 9 spectrum significantly cleans up the nitrocatechol peak at 422 nm (Fig. 1(iv)) which made it possible to quantify NDA functionalisation (Fig. S2.1†). Polymers were further characterised by ^{1}H NMR (Fig. S3.1†).

Several NDA-PNIPMAM polymers with different chain length were prepared (Table 1). Phase transition behaviour of NDA-PNIPMAM was studied using nano-differential scanning fluorimetry (NanoDSF), which can be used as small-scale turbidimetry. NanoDSF is well-suited for studying LCST as it detects the intensity of scattered light (at 280 nm) as a function of temperature with excellent temperature control. NDA-PNIPMAM showed concentration dependence of its phase transition (Fig. 1(v)). The LCST increased with decrease in the concentration of the polymer sample. This is consistent with literature reports on similar materials.[15,16] In the literature, LCSTs are usually reported either as the onset of the transition or as the temperature corresponding to the peak rate of scattering intensity change.[17,18] For our studies, the latter values are reported (Table 1). In addition to the concentration dependence of the LCST, we also observed an increase in the LCST with decreasing PNIPMAM molecular weight (Fig. 1(vi)). This molecular weight dependence of the polymer LCST is also consistent with literature reports.[4]

2.2. PNIPMAM coated IONPs

2.1.1. IONP synthesis. Iron oxide nanoparticles were prepared by adapting literature protocols for thermal decomposition of iron(III) acetylacetonate ($Fe(acac)_3$) in apolar organic solvents in the presence of ligands (Fig. 2).[19–22] All nanoparticle batches showed narrow size distributions. IONPs were soluble in organic solvents and hence were stored as toluene solutions at 4 °C.

2.1.2. Ligand exchange of IONPs with NDA-PNIPMAM. IONPs were functionalised with NDA-PNIPMAM using ligand exchange.[8,11] Excess polymer (in DMF) and IONPs (in toluene) were combined and sonicated for 5 h before stirring them overnight at room temperature. Polymer coated IONPs were purified using ultracentrifugation at 160 000*g* (22 °C). After purification, the nanoparticles were dispersed and stored in deionised water (dH_2O) at 4 °C. Polymer-coated IONPs showed excellent long-term stability, *e.g.*, no aggregation was observed after storage in physiological buffer at room temperature for 6 months (Fig. S4.2†).

PNIPMAM surface coverage of IONPs was estimated by thermogravimetric analysis (TGA) (Fig. 3(i)). Weight loss between 300 °C–450 °C corresponded to the amount of PNIPMAM present on the IONP surface.[8,11] We observed a gradual increase in the polymer weight loss with decrease in IONP size from 33 nm to 7 nm. For 19 kDa PNIPMAM, the grafting densities for each IONP size were 0.098 chains per nm^2 (7 nm), 0.062 chains per nm^2 (11 nm), 0.058 chains per nm^2 (16 nm), 0.032 chains per nm^2 (19 nm), 0.050 chains per

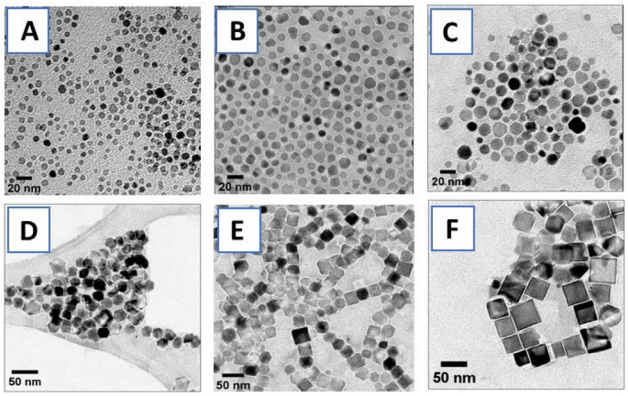

Fig. 2 Representative transmission electron microscopy (TEM) images of IONPs synthesized using thermal decomposition of $Fe(acac)_3$: (A) 7.3 ± 1.4 nm, (B) 11.0 ± 2.0 nm, (C) 15.4 ± 2.1 nm, (D) 19.1 ± 2.3 nm nano-octahedrals, (E) 27.4 ± 3.6 nm and (F) 33.4 ± 4.9 nm nanocubes (± denotes standard deviation, $n \geq 100$).

Table 1 Different chain length NDA-PNIPMAM synthesized *via* RAFT polymerization

M_w (kDa)	M_n/M_w	Yield (%)	LCST (°C)
4.7	2.9	70	50.5
19	3.2	80	45.9
86	8.3	76	44.6

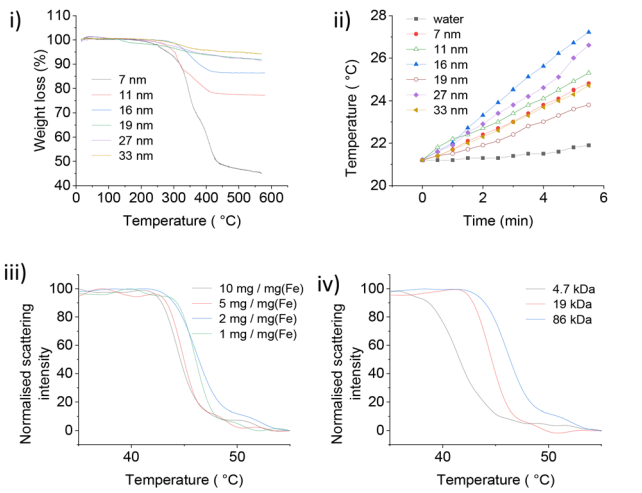

Fig. 3 (i) TGA analysis of 19 kDa PNIPMAM coated IONPs. 20 mg dry PNIPMAM coated IONPs were heated under air at a ramp rate of 10 °C min^{-1} between 0–600 °C. (ii) Magnetic heating curves for 19 kDa PNIPMAM @ IONPs. Magnetic heating measurement conditions: 0.45 ml of 10 mg ml^{-1} [Fe], AMF strength of 28.7 mT and frequency of 102.4 kHz. (iii) NanoDSF traces of 16 nm IONPs coated with 19 kDa PNIPMAM. (iv) NanoDSF traces of 16 nm IONPs coated with different chain length polymers. [Fe] = 1 mg ml^{-1}.

nm^2, (27 nm) and 0.034 chains per nm^2 (33 nm). These values are significantly lower than our previous report for 5 nm IONPs coated with 10 kDa PNIPAM (0.3 chains per nm^2).[8] The low grafting density of PNIPMAM could be attributed to the steric hindrance of the α-methyl groups and the increased polymer length. TEM images of PNIPMAM-coated IONPs (Fig. S4.1†) are similar to the uncoated ones (Fig. 2). Nanoparticles were also characterised by dynamic light scattering (DLS); hydrodynamic diameters and zeta potentials are given in Table 2 and section S5.†

The heating performance of PNIPMAM coated IONPs (Fig. 3 (ii)) was assessed by applying alternating magnetic field (AMF) at a constant voltage (30.0 V) and current (1.95 A) using a home-made equipment (section S6†).[8] To quantify and compare magnetic heating for different IONPs, specific absorption rate (SAR) values were calculated (Table 2).[8]

The SAR values of all IONPs were lower (Table 2) than many literature reports,[19–22] which was mainly due to the milder AMF conditions used in our study (magnetic field 28.7 mT, frequency 102.4 kHz, field-frequency product 2884.2 T s^{-1}). These parameters were designed to adhere to established human tolerance limits (6270 T s^{-1}),[23,24] and were similar to the clinical magnetic hyperthermia system approved for the treatment of prostate cancer (2257.2 T s^{-1}).[25] Unlike magnetic hyperthermia applications, protein release from PNIPMAM coated IONPs does not require a significant increase in the temperature of the bulk environment and so can be used with milder AMF parameters and lower SAR values.

Citrate (CA) coated IONPs were used as a benchmark (section S6†) to check the effect of polymer coating on the heating behaviour of IONPs. CA coated IONPs initially showed an increase in SAR with nanoparticle size (Table 2) from 6.1 W g^{-1} for 7 nm IONPs to 8.1 W g^{-1} for and 13.1 W g^{-1} for 11 nm and 16 nm IONPs, respectively. With further increase in size, SAR decreased to 4.7 W g^{-1} for 27 nm and 3.06 W g^{-1} for 33 nm nanocubes. In a related study, Mohapatra *et al.* also observed a bell-shape dependence of SAR with particle size, and maximum SAR was observed for 28 nm IONPs.[19] We also observed a similar size trend for PNIPMAM coated IONPs (Table 2), with 16 nm IONPs showing maximum heating performance (SAR = 7.5 W g^{-1}). The heating rate (SAR) of PNIPMAM coated IONPs was lower than that of citric acid coated IONPs.

Table 2 DLS data and SAR values of citric acid and 19 kDa PNIPMAM-coated IONPs

IONP core diameter (TEM) (nm)	Hydrodynamic diameter (nm)	Zeta potential (mV)	Citric acid IONP SAR (W g^{-1})	PNIPMAM IONP SAR (W g^{-1})
7	38	−18	6.1 ± 0.1	4.2 ± 0.3
11	52	−2.6	8.1 ± 0.3	5.0 ± 0.1
16	70	−1.9	13.1 ± 0.6	7.5 ± 0.1
19	80	−1.8	3.1 ± 0.3	2.5 ± 0.6
27	150	−1.0	4.7 ± 0.7	6.1 ± 0.7
33	180	−3.2	3.1 ± 0.4	3.9 ± 0.4

PNIPMAM coated IONPs also showed concentration dependence of their LCST, similar to pure polymer, however the dependence was much weaker (Fig. 3(iii) and 1(v)). This can be tentatively explained by the interactions between adjacent polymer chains adsorbed on the same particle, which is absent in dilute polymer solutions. This interaction does not depend on concentration, and hence the phase transition of PNIPMAM-coated particles does not show strong dependence on the concentration. Interestingly, the effect of PNIPMAM chain length on the LCST of free polymer and polymer-coated nanoparticles was opposite (Fig. 3(iv) and 1(vi)). LCST of PNIPMAM decreased with increasing polymer length. In contrast, LCST of PNIPMAM coated IONPs increased with increasing polymer chain length. This can also be attributed to the interactions between adjacent polymer chains attached to the same NP. In the particles coated with shorter polymers, all repeat units from different chains attached to the same particle are close to (and strongly interacting with) each other, essentially resembling a very high molecular weight polymer thus decreasing the LCST. However, for the longer polymer coated NPs, polymer chains protrude further into solution and behave independently, with weaker interactions between adjacent chains. For practical protein delivery applications, PNIPMAM-coated IONPs must have a phase transition onset at or above 45 °C to avoid significant protein leak at normal body temperature (37 °C). Hence, larger polymers (≥19 kDa, with LCST 43–46 °C) were used for further studies.

2.3. Protein–nanoparticle interactions

Understanding protein–nanoparticle interactions is critical for optimising protein encapsulation and release processes.[26–32] In our case, the polymer grafting density was low and hence the thickness of the polymer shell on the nanoparticle surface was also estimated to be low (*ca.* 2 nm for 19 kDa PNIPMAM @ 16 nm IONPs). Therefore, it was expected that the protein might interact with both the iron oxide core and the polymer shell.[33,34] These interactions could be of several different types. Proteins are negatively charged above and positively charged below their isoelectric point (pI). Zeta potential measurements of PNIPMAM coated IONPs revealed an overall negative surface charge (Table 2). There are no ionizable groups in the PNIPMAM repeat units at pH 7.4 and hence this negative charge would be on the IONP core leading to electrostatic interactions with charged proteins. Some amino acids (mainly histidine or cysteine) in the protein structure could bind to the metal oxide surface.[31] The amide functionalities in PNIPMAM repeat units can encapsulate protein by H-bonding. Below the LCST, the polymer chains on the IONP surface would be in the expanded form, which makes the polymer chains accessible for H-bonding with proteins. However, above the LCST, the polymer chains collapse to create a hydrophobic shell on the nanoparticle surface, which would lead to hydrophobic interactions with adsorbed proteins. Overall, protein encapsulation by PNIPMAM coated IONPs is likely to include contributions from a range of different types of non-covalent interactions (Fig. 4).

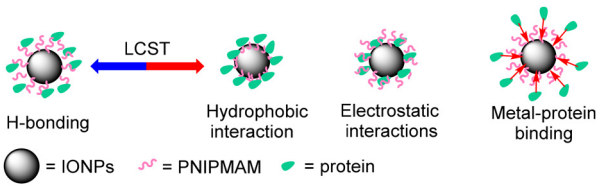

Fig. 4 Different types of protein-IONP interactions.

In order to get some information about the nature of protein–nanoparticle interactions, the effect of particle size and polymer chain length on the encapsulation/release of the model glycoprotein apotransferrin (TRF) was studied. Encapsulation was carried out by suspending the PNIPMAM-coated IONPs and the guest protein in a buffer at 45 °C followed by incubation at room temperature. While loading at high temperature could lead to partial denaturation of the guest protein, we found that this procedure is essential for successful loading and the following release of the protein guest, consistent with our previous observation.[8] A control experiment with model guest proteins showed no appreciable denaturation under these conditions (Fig. S12.1 and S12.2†).

Protein-loaded IONPs were stable in physiological buffer over a 24 h period. However visible precipitation appeared after 48 h storage, and TEM images showed aggregation after 1 week of storage (Fig. S4.3†). Protein-loaded IONPs were therefore used in subsequent experiments immediately after preparation.

2.4. Protein encapsulation/release studies

2.4.1. Effect of polymer chain length and nanoparticle size on TRF encapsulation/release. PNIPMAM coated IONPs were loaded with TRF by incubating a solution of protein and nanoparticles above the LCST (45 °C) before gradually cooling to room temperature.[8] The protein-loaded IONPs were subjected to multiple washes using a solution of the competitor protein RNaseB (10 mg ml^{-1}) below the LCST. This step aimed to eliminate any loosely attached guest protein and minimize subsequent protein leaching from the PNIPMAM coated IONPs. The quantification of protein encapsulation considered both the protein that remained unloaded and that which leached out during the washing process. After encapsulation, heat-triggered release of TRF was studied in the presence of the competitor protein RNaseB at high concentration (10 mg ml^{-1}) to mimic a biological environment, using immunoblotting to quantify protein loading and release.[8]

16 nm IONPs were used as a common core to study the effect of polymer chain length on protein encapsulation and release. TRF encapsulation increased with increasing chain length. When 0.5 mg of PNIPMAM coated IONPs was incubated with 1000 ng of TRF, only minimal protein loading was observed for 4.7 kDa (20 ng). However, as polymer chain length increased, protein encapsulation also increased, reaching 400 ng for 19 kDa polymer, and 700 ng for 86 kDa polymer. Increase in protein encapsulation with increasing polymer M_W suggests that encapsulation is at least partly driven by the interactions between proteins and polymer chains. After TRF encapsulation, its release was studied at 45 °C in the presence of RNaseB (Fig. 5(i)).

No protein release was observed for 4.7 kDa polymer coated IONPs, however 21 ng TRF was released at 45 °C with minimum leakage at 37 °C for 19 kDa PNIPMAM (Fig. 5(i)).

Further increase in M_W to 86 kDa led to an approximately 2-fold increase in triggered protein release. However, TRF leaching at 37 °C also increased to *ca.* 15 ng. The protein leak at 37 °C could be due to some protein loosely bound to IONPs functionalised with the longest polymer chains. This partial leak at 37 °C indicates the complexity of protein–nanoparticle interactions and underscores the importance of experimental validation of the encapsulation/release system. From these experiments we concluded that the 19 kDa PNIPMAM functionalised IONPs were the most advantageous for our further studies.

The effect of the IONP core diameter on protein encapsulation and release was studied with 7, 11 and 16 nm IONPs. 19 kDa PNIPMAM was used as a common coating and the same amount of IONPs (based on the mass of Fe) was used in these experiments. TRF encapsulation decreased with increasing NP diameter and maximum loading was observed for 7 nm IONPs (*ca.* 900 ng of 1000 ng TRF). This can be readily explained by the high surface area of smaller IONPs.

After TRF loading, we assessed release and found this to be strongly affected by the IONP size (Fig. 5(ii)). Despite higher protein encapsulation, only a small amount of TRF was released from 7 nm (*ca.* 7 ng) and 11 nm (*ca.* 5 ng) IONPs. However, 16 nm IONPs released *ca.* 21 ng at 45 °C with only a slight protein leak observed at 37 °C (*ca.* 1 ng). The smaller particles have higher curvature and hence likely a greater potential for the protein to irreversibly bind to iron oxide, which could be the reason for the observed lower protein release.

In conclusion, protein encapsulation increased with increased polymer chain length and decreased with IONP size. However, only 16 nm IONPs showed an appreciable temperature triggered protein release and hence 16 nm IONPs coated with 19 kDa PNIPMAM were used for all further studies.

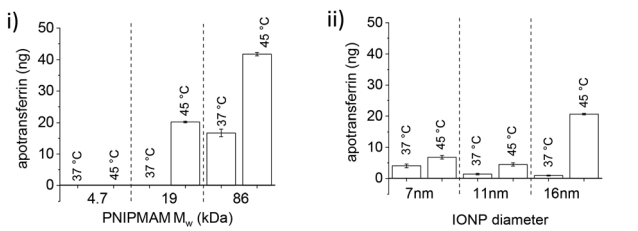

Fig. 5 Effect of (i) polymer chain length with 16 nm IONPs and (ii) IONP diameter with 19 kDa PNIPMAM, on heat-triggered TRF release. Western blot analysis and quantification of TRF release (with 10 mg ml^{-1} RNaseB) from PNIPMAM coated IONPs at 37 °C and 45 °C (for 1 h), respectively (n = 3, error bars denote standard error).

2.4.2. The effect of the physico-chemical properties of competitor proteins on protein release. In order to assess the relative importance of various physico-chemical properties of competitor proteins (Table 3) on protein release, heat-triggered TRF release was investigated in the presence of RNaseA, ovalbumin (OVL), bovine serum albumin (BSA) and bovine immunoglobulin (IgG). These proteins represent a range of sizes (from 15–160 kDa), surface charge states, and were chosen to have both glycosylated (RNaseB, ovalbumin, IgG) and non-glycosylated (RNaseA, BSA) examples given the significant extra hydrogen-bonding and chelating potential offered by the protein-linked glycan chains, and their mimicry of the proteins found in extracellular human bodily fluids.[35,36]

Following TRF encapsulation by PNIPMAM coated IONPs, release experiments with different glycosylated competitor proteins showed increased temperature-triggered TRF release with increasing competitor size. About 21 ng of the 400 ng loaded TRF was released with the 14.9 kDa RNaseB competitor and close to 175 ng with the 45 kDa OVL (Table 3). This increased release was accompanied by a slight increase in TRF leakage, which was dramatically increased when using an even larger protein, the 160 kDa IgG as a competitor. Thus, although IgG allowed releasing as much as 350 ng of the encapsulated TRF at 45 °C, leakage below the transition temperature amounted to almost a third of this. This can be explained by higher avidity of the bigger competitor proteins for IONPs. No clear effect of the competitor protein's pI was apparent in our experiments.

To test the effect of glycosylation on the TRF release we compared RNaseA and RNaseB as competitors. These two isoforms of RNase share the same polypeptide chains but only RNaseB is glycosylated.[42] Heat-triggered TRF release (Fig. 6) in the presence of RNaseA was only about 10% of the amount released in the presence of RNaseB. This is a strong indication that glycosylation significantly affects the interactions between proteins and polymer-coated IONPs above the LCST. This is presumably mediated through hydrogen bonding and/or chelating interactions of the multiple OH groups in the glycans with the iron oxide surface.

The importance of glycosylation for the effectiveness of the competitor protein was further confirmed in release experiments with the non-glycosylated competitor BSA (Fig. 6). Despite BSA having a larger size than OVL (66 *vs.* 45 kDa), the amount of TRF released by BSA was only about 20% (*ca.* 30 ng) of that released by OVL (*ca.* 175 ng). This is consistent with a significant effect of competitor glycosylation on heat-triggered protein release.

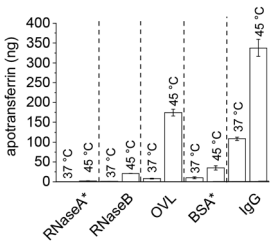

Fig. 6 Effect of competitor protein properties on heat-triggered TRF release. * = non-glycosylated proteins. Western blots are given in the ESI (section S7).†

To probe the specificity of this glycosylation effect, three monosaccharides (D-mannose, D-galactose and D-glucose) along with a disaccharide (maltose) and a polysaccharide (alginic acid) were used as competitors for heat-triggered TRF release, all at 10 mg ml^{-1} and pH 7.4. Only D-mannose resulted in a partial release of TRF above the LCST of PNIPMAM coated IONPs (Fig. S8.1†). Meng *et al.* found mannose to be a better chelator for iron compared to glucose and other sugars, which could explain our observation.[37] Additionally, the glycoproteins used in this study are mannose rich.[38,39] Specifically, RNaseB and OVL are primarily decorated with oligomannose structures, containing approximately 70–80% mannose, while IgG predominantly consists of complex glycans, with only about 30% mannose.[44] Based on these findings, it is plausible to suggest that the enhanced TRF release by glycosylated competitors could be attributed to mannose-IONP interactions. Furthermore, the size of the competitor may also play a role, as IgG, which has a lower proportion of mannose compared to RNaseB and OVL, showed increased TRF release.

2.4.3. The effect of guest protein size and glycosylation on encapsulation. The encapsulation and release of proteins from IONPs might depend not only on the properties of competitor proteins but also on those of the encapsulated guest protein. Assuming release is mainly governed by thermodynamic factors, guest protein properties should have an opposing effect compared to the competitor properties. To test this hypothesis, we studied the encapsulation and release of the small non-glycosylated green fluorescent protein (GFP, 27 kDa) alongside TRF and the larger glycosylated protein bovine IgG (160 kDa) using RNaseB and OVL as competitors. Consistent with prior trends, IgG exhibited higher encapsulation (approximately 800 ng of 1000 ng) than TRF (around 400 ng). On the other hand, GFP demonstrated an even better encapsulation efficiency (prior to washing), reaching about 900 ng.

After loading TRF and IgG, most of the loosely bound protein was removed with fewer than 10 competitor protein washes. However, GFP-loaded IONPs experienced significant protein loss during the initial RNaseB washes, followed by constant leakage with every subsequent wash below LCST. The

Table 3 Properties of guest and competitor proteins used in this study

Guest and competitor proteins	Molecular weight, kDa	Isoelectric point
RNaseA[a]	15	9.3
RNaseB	15	9.3
GFP[a]	27	6.2
OVL	45	5.2
BSA[a]	66	4.5
TRF	80	5.4
IgG	160	7.3

[a] Non-glycosylated proteins.

amount of protein leak was approximately three times higher when the larger OVL was used as a competitor (Fig. 7(i)). Heat-triggered GFP release with RNaseB or OVL did not differ significantly from the control experiment at 37 °C, suggesting that the small non-glycosylated GFP protein binds weakly to polymer-coated IONPs. In contrast, IgG's heat-triggered release with OVL as a competitor yielded a similar amount of protein as for TRF (about 150 ng, Fig. 7(ii)). However, there was a significant increase in the IgG leakage at 37 °C with the competitor OVL (*ca.* 30 ng) as compared to RNaseB (*ca.* 10 ng).

Finally, we investigated the kinetics of protein encapsulation by IONPs (Fig. 7(iii)). A range of glycosylated and non-glycosylated proteins used in this study (except GFP) showed similar loading behaviour with the saturation of the binding sites achieved within 60 min. More of the larger and glycosylated proteins was encapsulated as compared to the smaller and non-glycosylated ones, with GFP binding significantly faster than all other tested guest proteins.

Overall, protein encapsulation onto and release from PNIPMAM coated IONP is a complex process which depends on a number of physico-chemical properties of both the guest and competitor proteins. Both below and above the LCST, protein–nanoparticle interactions increased with glycosylation and increasing size of guest or competitor proteins. GFP, a small non-glycosylated protein, binds quickly but leaks out below the LCST, suggesting highly reversible binding.

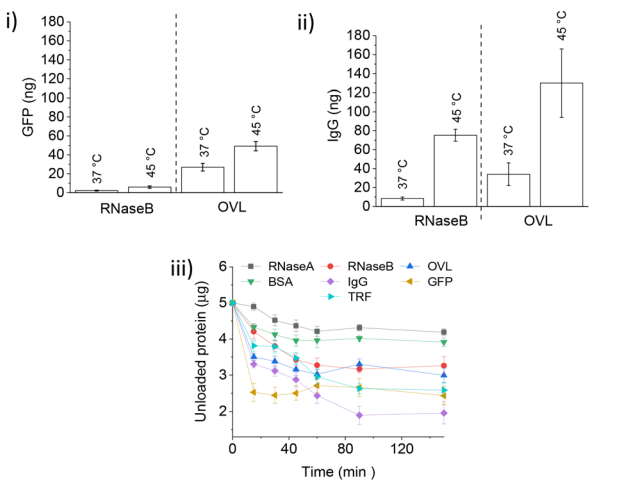

Fig. 7 (i) Heat-triggered release of GFP with different competitors. Quantification of GFP (Fig. S9.1†) release following competitor treatment for 60 min at 37 °C and 45 °C (RNaseB and OVL as indicated) of PNIPMAM coated IONPs loaded with 1000 ng GFP at pH 7.4 (n = 3, error bars denote standard error). (ii) Heat-triggered release of IgG with different competitors. Western blot analysis and quantification of IgG (section S10†) release following competitor treatment for 60 min at 37 °C and 45 °C (RNaseB and OVL as indicated) of PNIPMAM coated IONPs loaded with 1000 ng IgG at pH 7.4 (n = 3, error bars denote standard error). (iii) Protein encapsulation by IONPs at 22 °C: 0.5 mg PNIPMAM coated IONPs were mixed (350 rpm) with 5000 ng of the protein in the physiological buffer (20 mM HEPES, 100 mM NaCl, pH 7.4) (n = 3, error bars denote standard error). Protein quantification was done using Coomassie staining.

2.4.4. Investigating different temperature regimes for encapsulation. Guest protein leak below the LCST is likely to be due to some loosely bound protein. In order to maximise the amount of strongly bound protein and more completely remove the loosely bound guest, we tested different IgG loading/washing conditions (Fig. 8). Mixing PNIPMAM coated IONPs with the guest protein above the LCST (45 °C) for 15 min at the start of the encapsulation process before a 2 h incubation at room temperature was necessary for successful encapsulation, as incubating only at room temperature for 2 h completely eliminated temperature-responsive release above 45 °C (Fig. 8A and B). Importantly though, increasing the initial incubation time at 45 °C to 60 min significantly increased encapsulation, although this also somewhat increased leakage below the LCST (Fig. 8D, E and F). Variation of the length of incubation at 22 °C (following 15 min mixing at 45 °C) up to 2 h did not significantly affect encapsulation/release (Fig. 8B, C and E).

2.4.5. Serum as a competitor for magnetically-triggered IgG release. In any future *in vivo* applications of the coated IONPs, they will be exposed to a cocktail of proteins present in biological milieu.[40] In order to test whether this will provide a suitable environment for the release of the guest proteins, we explored guest protein release in the presence of serum as a potential source of competitor proteins. In order to quantify the release, we had to use guest proteins whose orthologs in various serums (bovine, goat and pig serum) would not interact with the antibody used for monitoring release (section S11†). For instance, TRF antigens in all three serums were detected by the antibodies used for the detection of human TRF. Hence, TRF release could not be quantified in the release experiments. However, the anti-bovine IgG antibody did not recognise the antibodies present in goat serum (section S11†). This system was therefore used in serum-triggered guest release experiments.

After IgG loading, treatment with goat serum as a competitor (10% in 20 mM HEPES, pH 7.4) during washings resulted in more protein leaching as compared to the OVL washings. The protein release with the serum was somewhat lower than with OVL as a competitor. At 45 °C, *ca.* 70 ng of IgG were released with a significant leakage of *ca.* 40 ng at 37 °C (Fig. 8 (B) and 9(i)). The protein concentration in serum is approxi-

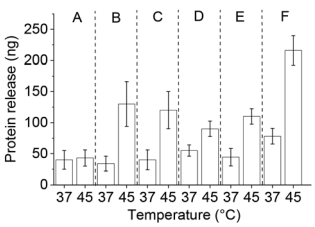

Fig. 8 Triggered IgG release with OVL as a competitor for different protein loading conditions: (A) 2 h at 22 °C (B) 15 min at 45 °C + 2 h at 22 °C (encapsulation procedure used throughout this study), (C) 15 min at 45 °C + 1 h at 22 °C, (D) 5 min at 45 °C, (E) 15 min at 45 °C and (F) 60 min at 45 °C.

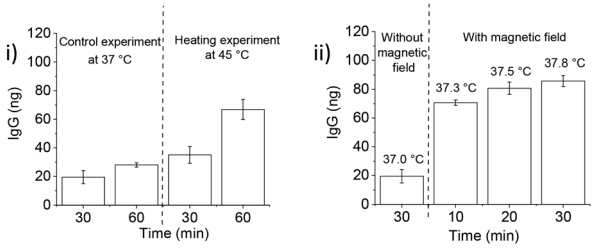

Fig. 9 IgG release from IONPs in a temperature-dependent manner. (i) Western blot analysis (section S11†) and quantification of IgG release following 10% goat serum treatment for 60 min at 37 °C and 45 °C of PNIPMAM coated IONPs loaded with 1000 ng IgG at pH 7.4 (n = 3, error bars denote standard error). (ii) Magnetic heating triggered IgG release from PNIPMAM @ IONPs at 37 °C: western blot analysis (section S11†) and quantification of IgG release following 10% goat serum treatment for 30 min at 37 °C with and without magnetic heating (10 s on/30 s off) of PNIPMAM coated IONPs loaded with 1000 ng IgG at pH 7.4 (n = 3, error bars denote standard error). Fe concentration 5 mg mL^{-1}, alternating magnetic field strength and frequency 28.7 mT and 102.4 kHz, respectively. Bulk solution temperatures measured during magnetic heating are provided above each timepoint. Protein release was calculated as the absolute amount of IgG associated with the particles after 10 washings.

mately 60–80 mg mL^{-1}, with 50–60% composed of albumins (*ca.* 60–70 kDa) and 40% of globulins, among which 10–20% are IgG (160 kDa).[45] These findings suggest that serum can serve as a potential source of competitor proteins for triggered protein release, but the issue of leakage below LCST still needs to be addressed.

The experiments carried out so far used conventional heating above the LCST to trigger guest protein release. Magnetic heating can lead to a different release profile as it affects the nanoparticle core much stronger than the surrounding medium. In order to assess suitability of the PNIPMAM coated IONP system for these applications, we explored magnetically-triggered release of IgG using serum as a competitor. AMF heating was applied in a pulsed sequence (10 s on–30 s off) to avoid heating of the bulk solution. Under these conditions, protein release after 30 min of magnetic heating was significantly higher (*ca.* 85 ng, Fig. 9(ii)) than with conventional heating (*ca.* 30 ng, Fig. 9(i)). Importantly, the bulk solution temperature stayed below the LCST of PNIPMAM coated IONPs (37.3 °C) during magnetic treatment. Protein leak at 37 °C in the absence of an AMF over a 30 min period was relatively small which suggests that the PNIPMAM coated IONP system can be used for delivery of therapeutic proteins using magnetic heating in a biological milieu acting as a source of competitor proteins.

3. Conclusions

We have successfully developed PNIPMAM-functionalised IONPs which could be used for the encapsulation and magnetically-triggered release of guest proteins. The polymer shell undergoes a phase transition above the LCST at *ca.* 45 °C, which makes the system suitable for *in vivo* applications. The PNIPMAM coated nanoparticles showed less pronounced dependence of LCST on polymer chain length than the free polymer. The IONPs with optimal particle size (*ca.* 16 nm) encapsulated and released guest proteins in the presence of a competitor protein. Protein–nanoparticle interactions showed complex dependence on protein properties, with stronger binding observed for larger and glycosylated proteins. Importantly, serum could be used as a physiologically relevant source of competitor proteins for guest release. Heat-triggered release experiments showed that some encapsulated protein leaches out below the LCST, but a significantly larger amount is released above the LCST. Magnetically-triggered heating released the encapsulated guest proteins at a faster rate than conventional heating, and without significant heating of the bulk solution. These observations show the potential of PNIPMAM coated IONPs for the delivery and magnetic release of therapeutic proteins in medicinal applications.

4. Experimental

4.1. Materials and methods

All chemicals and solvents were used as received unless mentioned otherwise. CTA was purchased from Fluorochem. Azobisisobutyronitrile (AIBN) was purchased from Sigma-Aldrich. Dopamine hydrochloride and sodium nitrite were purchased from Alfa Aesar. HBTU (2-(1*H*-benzotriazol-1-yl)-1,1,3,3-tetramethyluronium hexafluorophosphate) and *N*,*N*-diisopropylethylamine (DIPEA) were purchased from Sigma-Aldrich. Iron(III) acetylacetonate, oleylamine (OAm), 1,2-tertadecanediol, decanoic acid and benzyl ether were purchased from Sigma-Aldrich. Oleic acid (OA) and 4-biphenyl carboxylic acid were purchased from Alfa Aesar. Water used for lower critical solution temperature (LCST) studies was purified using a Millipore Milli-Q system with a QPAK 2 column. All syringe injections for water and air sensitive reactions were made using a syringe purged with nitrogen gas three times immediately prior to use. Proteins used in this study were purchased from Sigma Aldrich unless mentioned otherwise. All antibodies except anti bovine IgG (Bethyl) were purchased from Bio Rad.

4.2. General characterizations

UV-Vis spectroscopy was recorded on a Shimadzu UV-1800 UV-Vis spectrophotometer. ^{1}H-NMR (400 MHz) spectra were obtained in $CDCl_3$, D_2O or DMSO-d_6 using a JEOL ECS-400 spectrometer. Matrix-assisted laser desorption/ionisation-time of flight (MALDI-TOF) mass spectrometry was carried out on an Ultraflex spectrometer (Bruker) in positive linear ion mode. 1 mg mL^{-1} samples were spotted (2 μL) at dilutions of 1/10, 1/100 and 1/1000, made up in a 20 mg mL^{-1} matrix solution of alpha-cyano-4-hydroxycinnamic acid (CHCA) in THF. LCST of the polymer was determined by NanoDSF. Different concentrations of PNIPMAM were prepared in deionised water (dH_2O) (0.1–1 wt%) and loaded into the instrument in capillary tubes.

Temperature ramp rate was set to 0.4 °C min^{-1} and the scattering data were recorded from 20–75 °C. LCST was estimated by plotting first derivatives of the scattering intensity against temperature change. For the size determination of IONPs, TEM images were obtained using a JEOL 2011 transmission electron microscope operated at 200 kV accelerating voltage. Hydrodynamic diameter and zeta potential measurements were recorded using a Zetasizer and analysed using the DTS v. 5.1 supplied by Malvern. 1 mg mL^{-1} ([Fe]) samples were prepared by sonication in dH_2O for 15 min before placing sample (1 mL) into a disposable DLS cuvette for size distribution and a U-bend cell for zeta potential. Measurements were made at 25 °C, and carried out in triplicate at 10 runs per measurement. Molecular weight distributions of polymer samples were determined by gel permeation chromatography (GPC). Samples were prepared in pre-filtered methanol (2.5 mg cm^{-3}) and injected through three Agilent 8 μm Polargel columns (1 mL min^{-1}) maintained at 30 °C. This was then fed through Agilent UV (254 nm), refractive index, and viscometric (Agilent 1260 Infinity Detector Suite) detectors each maintained at 30 °C. The column was calibrated with linear PNIPAM standards.

4.3. Synthesis of PNIPMAM using RAFT

For a 1 g scale reaction, a mixture of *N*-isopropylmethacrylamide (NIPMAM) (1 g, 7.86 mmol) and isopropanol (1 mL) was heated to 70 °C until complete dissolution and cooled to room temperature. CTA (28.7 mg, 0.0786 mmol) in isopropanol (1 ml) was added to the NIPMAM solution and the reaction mixture was purged with Ar for 1 h. In a separate sample vial, a stock solution of AIBN in isopropanol (30.4 mM) was purged for 20 min under Ar. 200 μL (1 mg, 0.006 mmol) of this purged AIBN solution was added to the NIPMAM solution at 70 °C with vigorous stirring to start the polymerization. After 24 h, the reaction was quenched by cooling to room temperature. Solvent was removed on a rotary evaporator and the solid was dissolved in THF (5 ml). PNIPMAM was then selectively precipitated by adding *n*-pentane (40 ml) and the precipitates were collected by centrifugation (4500 rpm, 10 min). The precipitates were dissolved in THF and combined before evaporating the solvent on a rotary evaporator to get a solid product. Yield: 0.7 g (70%).^{1}H NMR: (D_2O, 400 MHz), ^{1}H NMR: (D_2O, 400 MHz), δ (ppm) = 6.9–7.3 (br m 1H), 3.6–3.9 (br m, 1H), 1.4–2.0 (br m, 2H), 0.5–1.1 (br m, 6H), 0.5–1.1 (br m, 3H). To synthesise polymers with M_w 4.7, 19 and 86 kDa, the following molar ratios of monomer : CTA : AIBN were used, respectively: 100 : 1 : 0.08; 400 : 1 : 0.3; 1000 : 1 : 0.8.

4.4. Conversion of PNIPMAM to NDA-PNIPMAM

Synthesis was adapted from a previous study.[11] PNIPMAM (2 g, 0.67 mmol, 3 kDa), HBTU (304.91 mg, 0.804 mmol) and DIPEA (116.7 μL, 0.67 mmol) were dissolved in dry DMF (19 mL) and purged with nitrogen gas for 15 min and stirred for 1 h. NDA (398.34 mg, 2.01 mmol) in DMF (1 mL) and DIPEA (233.4 μL, 1.34 mmol) were added under inert conditions, and the resulting solution was stirred at room temperature for 3 days. The solution was acidified with a few drops of 2 M HCl. The polymer was precipitated by dropping the solution in cold diethyl ether (100 ml) and collected *via* centrifugation (4500*g*, 10 min). The polymer was further purified by dissolving in a minimum volume of dH_2O (~10 ml) followed by centrifugation (4500*g*, 30 min) to remove unreacted NDA and dialysis (2 days), and dried on a rotary evaporator at 40 °C. Yield: 1.34 g (67%). ^{1}H NMR: (D_2O, 400 MHz), δ (ppm) = 7.5–7.6 (br m, 1H), 6.9–7.3 (br m, 1H), 6.6–6.7 (br m, 1H), 3.6–3.9 (br m, 1H), 13.48 (br m, 2H), 3.05 (br m, 2H), 1.4–2.0 (br m, 2H), 0.5–1.1 (br m, 6H), 0.5–1.1 (br m, 3H).

4.5 IONP synthesis

IONPs with diameter 7 nm were synthesized by following a recently developed colloidal synthesis route in which a mixture of $Fe(acac)_3$ (1.4 g, 4 mmol), 1,2-tetradecanediol (4.6 g, 20 mmol), oleic acid (6.78 g, 24 mmol) and oleylamine (6.4 g, 24 mmol) in benzyl ether (20.86 g) was refluxed at 300 °C to give monodisperse and highly crystalline IONPs.[20] The reaction mixture was magnetically separated (neodymium magnet) to yield black precipitates of IONPs which were redispersed in ethanol (10 ml) and reprecipitated by adding ethyl acetate (100 ml). The precipitated IONPs were magnetically separated and washed 3–5 times using ethanol/ethyl acetate washings. Washed IONPs were dispersed in toluene (5 ml) and stored at 4 °C. Similar washing procedure was used for the isolation, purification and storage of all the IONPs synthesized in this study. IONPs with average diameter 11 nm and 16 nm were obtained *via* a solvent-free $Fe(acac)_3$ thermal decomposition/reduction approach in oleylamine/oleic acid.[19] Iron oxide nano-octahedral (19 nm) and nanocubes (27 nm) were prepared by a modified literature approach.[21] For 19 nm nano-octahedral, $Fe(acac)_3$ (0.71 g, 4 mmol), oleic acid (2.82 g, 10 mmol), 4-biphenyl carboxylic acid (0.793 g, 4 mmol) and dibenzyl ether (20.8 g) were refluxed with an over-head stirrer. 27 nm IONPs were prepared as described for 19 nm octahedral IONPs using $Fe(acac)_3$ (1.4 g, 4 mmol), OA (2.54 g, 9 mmol), 4-biphenyl carboxylic acid (0.793 g, 4 mmol) and benzyl ether (20.8 g). The synthesis was done under magnetic stirring instead of using over-head stirrer. The nanocubes (40 nm) were obtained by refluxing a mixture of $Fe(acac)_3$ (0.353 g, 1 mmol) and decanoic acid (0.69 g, 4 mmol) in benzyl ether (25 ml).[22]

4.6. PNIPMAM coated IONPs

A toluene suspension (1 ml) of oleic acid/oleylamine (OA/OAm) capped IONPs (30 mg) and NDA-PNIPMAM (450 mg) were resuspended in DMF (5 ml). The reaction mixture was sonicated for 5 h at room temperature, and left overnight stirring. The polymer coated nanoparticles were then precipitated in diethyl ether (40 ml) and centrifuged (4500*g*, 15 min). The supernatant was removed and the particles were re-dissolved in dH_2O (10 ml). The unreacted polymer was removed using ultracentrifugation (160 000*g*, 1 h at room temperature). The precipitates were further washed 3–5 times by re-dissolving in

dH_2O and separation using Eppendorf centrifugation (20 000*g*, 30 min at room temperature). The washed precipitates were dissolved in dH_2O (3 ml) and stored at 4 °C. Yield: 20 mg (70%).

4.7. Determination of iron content in the IONPs

Total iron content of IONPs was determined using UV-Vis spectrophotometer.[41] The process was started with dissolving the known weight (5–10 mg) of IONPs in the minimum volume of conc. HCl (0.4 ml), resulting in the formation of a solution containing a mixture of Fe^{2+} and Fe^{3+} ions. The resulted solution was then diluted with dH_2O (25 ml) in a 50 ml volumetric flask and all the iron was then reduced to Fe^{2+} by adding excess of hydroxylamine hydrochloride (4 ml, 10 wt% in dH_2O). To this Fe^{2+} solution, *o*-phenanthroline (4 ml, 0.3 wt% in ethanol) was added resulting in the formation of an orange red complex (pH = 6–6.5) and the content of the iron was determined using the UV-Vis spectrophotometer (λ_{max} = 511 nm). The standard for the determination of the total iron content was Mohr salt.

4.8. Magnetic heating measurements

The heating performance of the water dispersible IONPs was assessed using an applied alternating magnetic field (magnetic field 28.7 mT, frequency 102.4 kHz, field-frequency product 2884.2 T s^{-1}) at a constant voltage (30.0 V) and current limit (1.95 A). A control experiment checked the background heating of deionised water (dH_2O). 0.45 ml dH_2O was loaded to a sample tube of dimensions 8 mm × 40 mm (diameter × height, Sigma) and the sample was put inside the heating chamber. Sample tube was held in a fixed position by a plastic holder and a lid was adapted to allow for insertion of thin plastic tubing for gallium arsenide thermocouple probe to monitor the temperature changes inside the chamber.[8] Magnetic heating data for various ligand coated IONPs were then recorded using above described procedure.

4.9. Preparation of protein-loaded nanoparticles

Prior to protein encapsulation, 0.5 mg of polymer-coated nanoparticles (100 μL, 5 mg ml^{-1} in dH_2O) were washed with 1 ml diethyl ether. Centrifugation (20 000*g*, 20 min) was used to separate washed IONPs. After ether washing, IONPs were washed three times by suspending in physiological buffer (1 ml) followed by centrifugation (20 000*g*, 20 min). After washing, IONPs were resuspended in 100 μl physiological buffer containing 1 μg guest protein. The solution was then incubated on a shaker at 45 °C for 15 min to agitate and suspend nanoparticles following precipitation at a temperature above polymer LCST (45 °C). IONPs were then incubated on a shaker at room temperature for 2 h. Particles were then separated using centrifugation, and the supernatant retained as the unloaded protein sample. Particles were then washed by suspending them in 100 μL of 10 mg mL^{-1} competitor protein solution in physiological buffer and incubating for 1 h at room temperature on a shaker. Particles were then separated using centrifugation and the supernatant was retained as first wash sample. This washing step was repeated multiple times (7–10), retaining each wash solution for further analysis.

4.10. Protein release assays

0.5 mg of protein-loaded, PNIPMAM coated IONPs were subjected to changes in temperature with or without magnetic heating. Experiments were conducted in 100 μL solutions of 10 mg mL^{-1} competitor protein in physiological buffer. To study triggered protein release above polymer LCST without magnetic heating, IONPs were resuspended in the competitor protein solution and incubated at 45 °C for 1 h. Between sampling time points IONPs were regularly agitated and at each sampling time point IONPs were magnetically separated before removing 10 μL of the sample volume for analysis. For magnetic heating experiment, pulsed AMF (10 s on–30 s off cycles) was used. 15 μl samples were collected and centrifuged to remove IONPs before collecting 10 μl supernatant for analysis.

4.11. Sample preparation for protein analysis

Following collection, protein samples were made up to 15 μL in SDS-PAGE sample buffer (5% (v/v) glycerol, 50 mM Tris-HCl pH 6.8, 50 mM dithiothreitol (DTT), 1% (w/v) sodium dodecyl sulfate (SDS), 0.7 mM Bromophenol Blue) and boiled at 97 °C for 5 min.

4.12. SDS-PAGE

SDS-PAGE gels were prepared according to the conditions reported in section S12.† For a separating gel composed of 10% (w/v) acrylamide, 375 mM pH 8.8 tris buffer, 0.05% (w/v) ammonium persulfate (APS) and 0.067% (w/v) *N*,*N*,*N*′,*N*′-tetramethylethylenediamine (TEMED), and a stacking gel containing 4% (w/v) acrylamide, 125 mM Tris pH 6.8, 0.1% (w/v) APS, 0.1% (w/v) TEMED. Samples were loaded into wells alongside 5 μL of a pre-stained protein ladder (Precision Plus All-Blue, Bio-Rad). Gels were placed in gel tanks and immersed in running buffer (25 mM Tris, 250 mM glycine, 0.1% (w/v) SDS) before running at 100 V constant voltage for 10 min and then at 150 V constant voltage until the dye had reached the bottom of the gel.

4.13. Coomassie staining

Fairbanks Coomassie staining[43] was carried out by heating gels in Fairbanks solution A (25% (v/v) isopropanol, 10% (v/v) acetic acid, 0.05% (w/v) Coomassie Brilliant Blue) to boiling before incubation for 5 min then washing with dH_2O. The heating and washing process was repeated with Fairbanks solution B (10% (v/v) isopropanol, 10% (v/v) acetic acid, 0.005% (w/v) Coomassie Brilliant Blue), Fairbanks solution C (10% (v/v) acetic acid, 0.002% (w/v) Coomassie Brilliant Blue) and Fairbanks solution D (10% (v/v) acetic acid). Gels were left in solution D until the background was completely destained. Quantification was carried out using ImageJ software after scanning the gels.

4.14. Western blotting

Western blotting was conducted by semi-dry transfer of gels onto PVDF membranes (Thermo Fisher) for 70 min at 0.3A using 48 mM Tris-HCl, 39 mM glycine, 20% (v/v) MeOH and 0.0375% (w/v) SDS as the transfer buffer. After membrane transfer, different blocking procedures were used for TRF and IgG. For TRF, membranes were blocked using phosphate buffered saline (PBS) with 0.05% (v/v) Tween-20 (PBST) and 5% (w/v) dried fat free milk powder (PBSTM) for 1 h at room temperature. Membranes were then incubated with primary antibody: anti-TRF (1 : 500, Dako) in PBSTM solution overnight at 4 °C. Following six 10 min washes at room temperature in PBSTM solution, goat anti rabbit-horseradish peroxidase (1 : 1000, Bio-Rad) secondary antibody in PBSTM solution was added for 1 h at room temperature. The blot was then washed 3 times with PBSTM solution (5 min each) and 3 times in PBST for 10 min each at room temperature. For IgG, membranes were blocked in tris-buffered saline (TBS) with 0.05% (v/v) Tween-20 (TBST) and Roche blocking solution (1 : 10) for 1 h at room temperature. Membranes were then incubated with goat anti bovine IgG-horseradish peroxidase (1 : 250) for 1 h followed by three 5 min washings with blocking solution followed by three 10 min TBST washings. Blots were imaged on an Invitrogen iBright imaging system after application of Immobilon horseradish peroxidase (HRP) substrate (Millipore). Quantification was carried out using ImageJ software.

Conflicts of interest

There are no conflicts to declare.

Acknowledgements

The authors acknowledge the University of York and Wild fund for funding this project. Dr I. Will (University of York) is gratefully acknowledged for supporting magnetic heating experiments.

References

1 J. Zhang and R. D. K. Misra, *Acta Biomater.*, 2007, **3**, 838–850.
2 R. K. Dani, C. Schumann, O. Taratula and O. Taratula, *AAPS PharmSciTech*, 2014, **15**, 963–972.
3 T. Hoare, J. Santamaria, G. F. Goya, S. Irusta, D. Lin, S. Lau, R. Padera, R. Langer and D. S. Kohane, *Nano Lett.*, 2009, **10**, 3651–3657.
4 J. Rathfon and G. Tew, *Polymer*, 2008, **49**, 1761–1769.
5 R. Shunmugam and N. G. Tew, *Polymer*, 2005, **43**, 5831–5843.
6 M. Giannaccini, M. P. Calatayud, A. Poggetti, S. Corbianco, M. Novelli, M. Paoli, P. Battistini, M. Castagna, L. Dente, P. Parchi, M. Lisanti, G. Cavallini, C. Junquera, G. Goya and V. Raffa, *Adv. Healthcare Mater.*, 2017, **6**, 1601429.
7 D. Maity, S. N. Kale, K. R. Ghanekar, M. J. Xue and J. Ding, *J. Magn. Magn. Mater.*, 2009, **321**, 3093–3098.
8 M. Walker, I. Will, A. Pratt, V. Chechik, P. Genever and D. Ungar, *ACS Appl. Nano Mater.*, 2020, **3**, 5008–5013.
9 R. T. A. Mayadunne, E. Rizzardo, J. Chiefari, J. Krstina, G. Moad, A. Postma and S. H. Thang, *Macromolecules*, 2000, **33**, 243–245.
10 J. V. John, C. W. Chung, R. P. Johnson, Y. I. Jeong, K. D. Chung, D. H. Kang, H. Suh, H. Chen and I. Kim, *Biomacromolecules*, 2016, **17**, 20–31.
11 S. Kurzhals, R. Zirbs and E. Reimhult, *ACS Appl. Mater. Interfaces*, 2015, **7**, 19342–19352.
12 J. S. Kim, T. G. Kim, W. H. Kong, T. G. Parka and Y. S. Nam, *Chem. Commun.*, 2012, **48**, 9227–9229.
13 M. Arslan, T. N. Gevrek, J. Lyskawa, S. Szunerits, R. Boukherroub, R. Sanyal, P. Woisel and A. Sanyal, *Macromolecules*, 2014, **47**, 5124–5134.
14 K. Skrabania, A. Miasnikova, A. M. B. Koumba, D. Zehm and A. Laschewsky, *Polym. Chem.*, 2011, **2**, 2074–2083.
15 C. Boutris, E. G. Chatzi and C. Kiparissides, *Polymer*, 1998, **38**, 2567–2570.
16 F. Afroze, E. Nies and H. Berghmans, *J. Mol. Struct.*, 2000, **554**, 55–68.
17 K. Otake, H. Inomata, M. Konno and S. Saito, *Macromolecules*, 1990, **23**, 283–289.
18 H. G. Schild and D. A. Tirrell, *J. Phys. Chem.*, 1990, **94**, 4352–4356.
19 J. Mohapatra, Z. Fanhao, K. Elkins, M. Xing, M. Ghimire, S. Yoon, S. R. Mishra and J. P. Liu, *Phys. Chem. Chem. Phys.*, 2018, **20**, 12879–12887.
20 S. Tong, C. A. Quinto, L. Zhang, P. Mohindra and G. Bao, *ACS Nano*, 2017, **11**, 6808–6816.
21 D. Kim, N. Lee, M. Park, B. H. Kim, K. An and T. Hyeon, *J. Am. Chem. Soc.*, 2009, **131**, 454–455.
22 P. Guardia, R. D. Corato, L. Lartigue, C. Wilhelm, A. Espinosa, M. G. Hernandez, F. Gazeau, L. Manna and T. Pellegrino, *ACS Nano*, 2012, **6**, 3080–3091.
23 W. J. Atkinson, I. A. Brezovich and D. P. Chakraborty, *IEEE Trans. Biomed. Eng.*, 1984, **31**, 70–75.
24 R. Hergt and S. Dutz, *J. Magn. Magn. Mater.*, 2007, **311**, 187–192.
25 U. Gneveckow, A. Jordan, R. Scholz, V. Brüss, N. Waldöfner, J. Ricke, A. Feussner, B. Hildebrandt, B. Rau and P. Wust, *Med. Phys.*, 2004, **31**, 1444–1451.
26 H. Mok and M. Zhang, *Expert Opin. Drug Delivery*, 2013, **10**, 73–87.
27 P. M. Price, W. E. Mahmoud, A. A. Al-Ghamdi and L. M. Bronstein, *Front. Chem.*, 2018, **11**, 1–7.
28 R. K. Dani, C. Schumann, O. Taratula and O. Taratula, *AAPS PharmSciTech*, 2014, **15**, 963–972.
29 N. Pandey, J. U. Menon, M. Takahashi, J. T. Hsieh, J. Yang, K. T. Nguyen and A. S. Wadajkar, *Nanotheranostics*, 2020, **4**, 1–13.

30 M. A. C. Stuart, W. T. S. Huck, J. Genzer, M. Müller, C. Ober, M. Stamm, G. B. Sukhorukov, I. Szleifer, V. V. Tsukruk, M. Urban, F. Winnik, S. Zauscher, I. Luzinov and S. Minko, *Nat. Mater.*, 2010, **9**, 101–113.
31 D. Chakraborty, K. R. Ethiraj and A. Mukherjee, *RSC Adv.*, 2020, **10**, 27161–27172.
32 W. J. Jeong, J. Yu and W. J. Song, *Chem. Commun.*, 2020, **56**, 9586–9599.
33 N. Zhang, X. Shen, K. Liu, Z. Nie and E. Kumacheva, *Acc. Chem. Res.*, 2022, **55**, 1503–1513.
34 M. A. Firestone, S. C. Hayden and D. L. Huber, *MRS Bull.*, 2015, **40**, 760–767.
35 M. Ardejani, L. Noodleman, E. Powers and J. Kelly, *Nat. Chem.*, 2021, **13**, 480–487.
36 Z. Ghanbari, M. R. Housaindokht, M. R. Bozorgmehr and M. Izadyar, *J. Theor. Biol.*, 2016, **404**, 73–81.
37 K. Meng, C. Yao, Q. Ma, Z. Xue, Y. Du, W. Liu and D. Yang, *Adv. Sci.*, 2019, **6**, 1802112.
38 J. Prien, D. Ashline, A. Lapadula, H. Zhang and V. Reinhold, *J. Am. Soc. Mass Spectrom.*, 2009, **20**, 539–556.
39 L. Lang, R. Couso and S. Kor, *J. Biol. Chem.*, 1986, **261**, 6320–6325.
40 M. Leeman, J. Choi, S. Hansson, M. U. Storm and L. Nilsson, *Anal. Bioanal. Chem.*, 2018, **410**, 4867–4873.
41 H. Khurshid, J. Alonso, Z. Nemati, M. H. Phan, P. Mukherjee, M. L. F. Gubieda, J. M. Barandiar and H. Srikanth, *J. Appl. Phys.*, 2015, **117**, 17A3371–17A3374.
42 H. C. Joao, I. G. Scragg and R. A. Dwek, *FEBS Lett.*, 1992, **307**, 343–346.
43 G. Fairbanks, T. L. Steck and D. F. Wallach, *Biochemistry*, 1971, **10**, 2606–2617.
44 S. Boune, P. Hu, A. L. Epstein and L. A. Khawli, *Antibodies*, 2020, **9**, 1–20.
45 M. Leeman, J. Choi, S. Hansson, M. U. Storm and L. Nilsson, *Anal. Bioanal. Chem.*, 2018, **410**, 4867–4873.